Journal of Hydrology 526 (2015) 183–195

Contents lists available at ScienceDirect

Journal of Hydrology

journal homepage: www.elsevier.com/locate/jhydrol

Droughts in a warming climate: A global assessment of Standardized precipitation index (SPI) and Reconnaissance drought index (RDI)

Mohammad Amin Asadi Zarch [a], Bellie Sivakumar [a,b,*], Ashish Sharma [a]

[a] School of Civil and Environmental Engineering, The University of New South Wales, Sydney, NSW 2052, Australia
[b] Department of Land, Air and Water Resources, University of California, Davis, CA 95616, USA

ARTICLE INFO

Article history:
Available online 5 October 2014

Keywords:
Drought
Aridity
Standardized precipitation index
Reconnaissance drought index
Climate change

SUMMARY

Both drought and aridity indicate imbalance in water availability. While drought is a natural temporal hazard, aridity is a constant climatic feature. This paper investigates the changes in drought characteristics across different aridity zones with and without consideration of potential evapotranspiration (PET), as a means to better assess drought in a warming climate. Two drought indexes are employed: (1) Standardized precipitation index (SPI), which is solely based on precipitation; and (2) Reconnaissance drought index (RDI), which, in addition to precipitation, takes PET into account. The two indexes are first employed to observed precipitation and PET data for the period 1960–2009 from the CRU (Climate Research Unit, University of East Anglia) TS 3.1 database. The results indicate that although all the aridity zones experience both downward and upward drought trends, no significant trend is found over large parts of the zones. However, the agreement between SPI and RDI reduces from the hyper-arid zone on one extreme toward the humid zone on the other. In the three more humid zones (i.e. semi-arid, sub-humid, and humid), the indexes exhibit different trends, with RDI showing more decreasing trends (i.e. becoming drier). While SPI generally shows more drought prone areas than RDI for the pre-1998 period, the opposite is observed for the post-1998 period. Given the known changes to PET in observed records, and also expected increases as global warming intensifies, these results suggest that RDI will be consistently different to the SPI as global warming intensifies. This hypothesis is further tested for historic and future climate projections from the CSIRO (Commonwealth Scientific and Industrial Research Organisation, Australia) Mk3.6 global climate model (GCM), with use of the fifth phase of the Coupled Model Intercomparison Project (CMIP5) and RCP8.5 (Representative Concentration Pathways). In this case, PET is calculated using FAO56-PM model for assessment of RDI. The results suggest that agreement between SPI and RDI is affected and decreases remarkably over time (between 1850 and 2100). All these lead to the conclusion that, in the face of climate change, PET, an important component in the hydrologic cycle, should not be ignored in drought modeling.

1. Introduction

Population growth, better living standards, increase in agricultural and industrial activities, degradation in water quality, and many other factors continue to influence and increase our demands for freshwater around the globe. The significant spatial and temporal variability of water resources often result in water deficiencies in different regions and at different times. As a result, water planning and management is often a challenging task in many regions, and has the potential to lead to conflicts between different stakeholders (e.g. nations, water use sectors); see, for example, Sivakumar (2011a) for a recent account. This problem becomes far more complicated during periods of droughts. It is particularly in this context that there are serious concerns about the impacts of climate change on our water security, socio-economic development, and environmental sustainability, since climate change is anticipated to result in increases in the frequency, duration, and severity of droughts (and other hydroclimatic extremes). It is also reasonable to assume that the impacts of climate change will be realized far more in the arid (hyper-arid, arid, and semi-arid) regions, where the availability of rainfall and soil moisture is already very low.

Drought is a natural and recurring feature of climate, and occurs in virtually all climatic regimes; see Mishra and Singh (2010, 2011)

* Corresponding author at: School of Civil and Environmental Engineering, The University of New South Wales, Sydney, NSW 2052, Australia. Tel.: +61 2 93855072; fax: +61 2 93856139.
E-mail address: s.bellie@unsw.edu.au (B. Sivakumar).

http://dx.doi.org/10.1016/j.jhydrol.2014.09.071
0022-1694/

for comprehensive reviews of drought concepts and modeling. The primary cause of any drought is a deficiency in rainfall and, in particular, the timing, distribution, and intensity of this deficiency in relation to the existing water storage, demand, and use. Therefore, drought is a prolonged period of water deficit, and typically occurs when an area receives precipitation below usual levels for several months (Gocic and Trajkovic, 2014). There are three well-known types of drought: (1) meteorological or climatological drought; (2) hydrological drought; and (3) agricultural or vegetative drought (Tallaksen and van Lanen, 2004). Meteorological drought results from a shortage of precipitation, and can be defined as a drying relative to the mean state. Hydrological drought follows meteorological drought, and is a deficiency in the volume of water supply. Agricultural or vegetative drought occurs when, because of insufficient soil moisture, supply of moisture for crops reduces. With regard to the existence of different types of drought, a wide range of drought identification and assessment indexes have been introduced in the literature, including: Palmer drought severity index (PDSI) (Palmer, 1965); Surface water supply index (SWSI) (Shafer and Dezman, 1982); Standardized precipitation index (SPI) (McKee et al., 1993); Reconnaissance drought index (RDI) (Tsakiris and Vangelis, 2005); and copula-based joint deficit index (JDI) (Kao and Govindaraju, 2010). The indexes have also been used in different contexts (e.g. Chen and Chan, 2007; Özger et al., 2010). These indexes usually depend on some combination of precipitation, temperature, potential evaporation (PE) or potential evapotranspiration (PET), soil moisture and/or streamflow. Each of these indexes is relevant to a specific type of drought.

It is important to point out that the concept of drought is sometimes not properly distinguished from that of aridity. As a result, both drought and aridity are sometimes considered synonymous and treated in the same way. For example, areas suffering from drought may not be recognized properly from regions with simply arid or hyper-arid climatic features. The fact that both drought and aridity can be defined from similar parameters (e.g. precipitation, available water or humidity) only adds to this confusion. However, there is an important difference between the two. Drought is a natural hazard, and is essentially a temporal anomaly from normal conditions. Aridity, on the other hand, is a climatic feature, and is a constant imbalance in the water availability consisting of low average annual precipitation, with high spatial and temporal variability, resulting in overall low moisture and low carrying capacity of the ecosystems (Sanderson, 1992). While statistical indexes defined as anomalies from normal conditions are useful when investigating droughts, absolute methods must be considered in the definition of arid climate regions (Damberg, 2013).

The effects of climate change are global in scope and vary from region to region, and thus have important implications for hydrology (especially extremes) and water resources at global, regional, and local scales; see, for example, Mishra and Singh (2009), Sivakumar (2011b), and Yang and Yang (2012) for comprehensive accounts of the challenges in assessing the impacts of climate change on water resources. Since drought is a regional phenomenon, the impacts of climate change on droughts may differ across the world. Therefore, on one hand, it can be presumed that drought occurrence and trends exhibit various patterns in different climatic features or aridity zones. On the other hand, although all the aridity zones are relatively vulnerable to droughts, the potency of each zone to confront droughts is different. For instance, under the same level of severity of drought, arid zones are in a more vulnerable position when compared to humid zones. Therefore, finding general patterns and tendencies of droughts in each climatic zone is important for a more accurate assessment of climate change impacts on water resources. This provides the motivation for the present study.

The objective of this paper is to assess the spatio–temporal variation trends of drought events in different climatic zones (defined by aridity) around the globe. Two drought indexes are employed: the Standardized precipitation index (SPI), and the Reconnaissance drought index (RDI). The SPI, arguably a more popular drought index, is based solely on precipitation, and measures how much precipitation for a given period of time has deviated from historically established norms. The RDI uses PET, in addition to precipitation, as a key variable for assessing the severity of drought. It is hypothesized that the outcomes from the use of these two indexes will become increasingly different as the assessment focused on a warmer climate where PET can be expected to increase (Johnson and Sharma, 2010). To put the analysis in a proper perspective, the two indexes are first employed to past observed data from the CRU (Climate Research Unit, University of East Anglia) TS 3.1 database, and their performances are compared for an informed assumption on their capability to represent droughts. This assumption and also the hypothesis that the outcomes will increasingly differ in markedly warmer climates are then tested on raw historic and future simulations from the CSIRO (Commonwealth Scientific and Industrial Research Organisation, Australia) Mk3.6 global climate model (GCM), with use of the fifth phase of the Coupled Model Intercomparison Project (CMIP5) (Taylor et al., 2012).

The rest of this paper is organized as follows. Section 2 describes the data and methodology used. Section 3 presents the results, with particular emphasis on the drought trends in different aridity zones and SPI and RDI relationships in the past and future. Section 4 discusses the results, followed by a set of conclusions in Section 5.

2. Materials and methods

In this study, precipitation observations and PET data derived from real observations are used to obtain SPI and RDI time series and to identify droughts during the last five decades (1960–2009) worldwide. The Mann–Kendall test is applied to detect probable trends and (dis)similarities in the SPI and RDI series. The findings are then examined for the future through CMIP5 simulations. The datasets and methods used here are described below.

2.1. Observed data

This study uses high spatial resolution ($0.5^\circ \times 0.5^\circ$) gridded monthly data CRU TS 3.1, an observational data source, from the Climatic Research Unit, University of East Anglia. The CRU TS 3.1 dataset covers the period 1901–2009 and data are available over land areas excluding Antarctica. The CRU TS3.1 provides a monthly time series of global gridded data based on observations from more than 4000 stations (Belda et al., 2014). The dataset includes six mostly independent climate variables (mean temperature, diurnal temperature range, precipitation, wet-day frequency, vapor pressure, and cloud cover). Maximum and minimum temperatures are arithmetically derived from these. Secondary variables (frost day frequency and PET) are estimated from the six primary variables (Harris et al., 2014). The method used here for the calculation of PET is a variant of the Penman–Monteith formula (see Harris et al., 2014).

2.2. Drought indexes

2.2.1. Standardized precipitation index (SPI)

Computation of the SPI involves fitting a gamma probability density function (PDF) to a given time series of precipitation. This is performed separately for each month (or any other temporal basis of the raw precipitation time series) and for each location

in space. The gamma distribution is defined by its probability density function as:

$$g(x_k) = \frac{1}{\beta^{\alpha}\Gamma(\alpha)} x_k^{\alpha-1} e^{-x_k/\beta} \quad for \ : \ x_k > 0 \tag{1}$$

where $\alpha > 0$ is a shape factor, $\beta > 0$ is a scale factor, and $x_k > 0$ is the amount of precipitation over k consecutive months, represented as $x_k^{(i)} = \sum_{j=1}^{k} P_{ij}$, $i = 1$ to N, where P_{ij} is the precipitation of the j-th month of the i-th year and N is the total number of years of the available data. The function $\Gamma(\alpha)$, here, is the gamma function, given as:

$$\Gamma(\alpha) = \int_0^{\infty} y^{\alpha-1} e^{-y} dy \tag{2}$$

Fitting the distribution to the data requires α and β to be estimated. Using the approximation of Thom (1958), these parameters can be estimated as follows:

$$\alpha = \frac{1}{4A}\left(1 + \sqrt{1 + \frac{4A}{3}}\right) \tag{3}$$

$$\beta = \frac{\overline{x_k}}{\alpha} \tag{4}$$

where

$$A = \ln(\overline{x_k}) - \frac{1}{n}\sum_{i=1}^{n} \ln((x_k)_i) \tag{5}$$

for n observations.

Integrating the probability density function with respect to x_k yields the following expression $G(x_k)$ for the cumulative probability:

$$G(x_k) = \int_0^{x_k} g(x_k) dx_k = \frac{1}{\beta^{\alpha}\Gamma(\alpha)} \int_0^{x_k} x_k^{\alpha-1} e^{-x_k/\beta} dx_k \tag{6}$$

Substituting t for $\frac{x_k}{\beta}$ reduces Eq. (6) to an incomplete gamma function

$$G(x_k) = \frac{1}{\Gamma(\alpha)} \int_0^{x_k} t^{\alpha-1} e^{-t} dt \tag{7}$$

The gamma distribution is undefined for $x_k = 0$. Since precipitation distribution may contain zeros, in order to account for zero value probability, the cumulative probability may be written as:

$$H(x_k) = q + (1-q)G(x_k) \tag{8}$$

where q is the probability of zero precipitation. The cumulative probability, $H(x_k)$, is then transformed to the standard normal random variable Z with mean zero and variance one, which is the value of SPI. Following the approximate conversion provided by Abramowitz and Stegun (1965), Z, and hence SPI, is expressed as:

$$Z = SPI = -\left(t - \frac{c_0 + c_1 t + c_2 t^2}{1 + d_1 t + d_2 t^2 + d_3 t^3}\right), \quad t = \sqrt{\ln\left(\frac{1}{H(x_k)^2}\right)} \quad for\, 0 < H(x_k) < 0.5 \tag{9}$$

and

$$Z = SPI = \left(t - \frac{c_0 + c_1 t + c_2 t^2}{1 + d_1 t + d_2 t^2 + d_3 t^3}\right), \quad t = \sqrt{\ln\left(\frac{1}{(1 - H(x_k))^2}\right)} \quad for\, 0.5 < H(x_k) < 1.0 \tag{10}$$

with $c_0 = 2.515517$, $c_1 = 0.802853$, $c_2 = 0.010328$, $d_1 = 1.432788$, $d_2 = 0.189269$, and $d_3 = 0.001308$. Positive SPI values indicate greater than median precipitation, and negative values indicate less than median precipitation. Since SPI is normalized, wetter and drier climates can be represented in the same way, and wet periods can also be monitored using SPI.

2.2.2. Reconnaissance drought index (RDI)

The RDI can be expressed in three forms: the initial value (a_k), normalized RDI (RDI_n), and standardized RDI (RDI_{st}). The initial value (a_k) is presented in an aggregated form using a monthly timestep and may be calculated on a monthly, seasonal or annual basis. It is calculated in a time basis of k (months) using the following equation:

$$a_k^{(i)} = \frac{\sum_{j=1}^{k} P_{ij}}{\sum_{j=1}^{k} \mathrm{PET}_{ij}}, i = 1 \text{ to } N \tag{11}$$

where P_{ij} and PET_{ij} are precipitation and PET of the j-th month of the i-th year and N is the total number of years of the available data. The normalized RDI (RDI_n) is computed using:

$$\mathrm{RDI}_{n(k)}^{(i)} = \frac{a_k^{(i)}}{\bar{a}_k} - 1 \tag{12}$$

where $\bar{a}_k$ is the arithmetic mean of a_k values. The initial formulation of the standardized RDI (RDI_{st}) (Tsakiris and Vangelis, 2005) used the assumption that a_k values follow the lognormal distribution, and thus:

$$\mathrm{RDI}_{st(k)}^{(i)} = \frac{y_k^{(i)} - \bar{y}_k}{\hat{\sigma}_{yk}} \tag{13}$$

where y_k is $\ln(a_k^{(i)})$, $\bar{y}_k$ is the arithmetic mean of y_k and $\hat{\sigma}_{yk}$ is its standard deviation. However, through analysis of various data from several locations and different timescales, it has been shown that, although a_k values follow both lognormal and gamma distributions, gamma distribution shows the best fit in most locations and timescales (Tsakiris et al., 2008). Therefore, the calculation of RDI_{st} could be performed better by fitting the gamma probability density function to the given frequency distribution of a_k, following the procedure described below. Similar to the SPI computation by the gamma approach, this approach also solves the problem of calculating RDI_{st} for small timesteps, such as monthly, which may include zero-precipitation values ($a_k = 0$), for which Eq. (13) cannot be applied (Tsakiris et al., 2008). For this purpose, the RDI calculation is the same as that for SPI and Eqs. (1)–(10) can be applied by replacing x_k by a_k values. The present study employs this method to assess RDI. For this study, x_k (to ascertain SPI) and a_k (to assess RDI) values are aggregated over the same temporal window. For the purposes of the trend assessments reported later, k is assumed equal to 12, such that both SPI and RDI represent annual aggregated values. As SPI and RDI_{st} perform in a similar manner, their results can be interpreted in a similar manner as well. Therefore, the values of RDI_{st} could be compared to the same thresholds as that of the SPI technique, as shown in Table 1.

Table 1
Drought classification according to SPI and RDI Values.

SPI and RDI range	Drought classes
2 or more	Extremely wet
1.5–1.99	Very wet
1–1.49	Moderately wet
0.99–0.0	Normal
0.0 to −0.99	Near normal
−1 to −1.49	Moderately dry
−1.5 to −1.99	Severely dry
−2 and less	Extremely dry

2.3. Mann–Kendall test

In this study, in order to detect the significant trends in SPI and RDI time series, the Mann–Kendall test, developed by Mann (1945) and Kendall (1975), is used. Testing the significance of observed trends in hydrologic and climatic time series has received a great deal of attention recently. The rank-based Mann–Kendall (MK) test is the most widely used nonparametric method for trend detection. Being a nonparametric test, the MK test can be applied to data no matter what the probability distribution is. Distribution-free tests have the advantage that their power and significance are not affected by the actual distribution of the data. This is in contrast to parametric trend tests, such as the regression coefficient test, which assume that the data follow the Normal distribution, and so their power can be greatly reduced in the case of skewed data (Hamed, 2009).

Consider a time series $\{X_i | i = 1, 2, ..., N\}$ with a record length N. According to Salas (1993) and Yu et al. (1993), the null hypothesis H_0 states that the data $\{X_i\}$ are a sample of n independent and identically distributed (iid) random variables. The alternative hypothesis (H_1) of a two-sided test is that the distribution of X_i and X_j are not identical for $i, j \leqslant N$ with $i \neq j$. Each value $X_i = 1, 2, \ldots, N-1$ is compared with all subsequent values of $\{X_j | j = i+1, i+2, ..., N\}$ and sum of the times of $X_i > X_j$. The number of positive differences for all the differences considered, p, is given by:

$$p = \sum_i n_i \tag{14}$$

The Mann–Kendall statistic, S, is calculated as:

$$S = \left(\frac{4p}{(N(N-1))}\right) - 1 \tag{15}$$

Under the H_0 hypothesis, the distribution of S is normal in the limit as $N \to \infty$ (Yu et al., 1993). The mean and variance of S are calculated as:

$$E(S) = 0 \tag{16}$$

$$Var(S) = 2(2N+5)/(9N(N-1)) \tag{17}$$

For $N > 10$, the test is conducted using a normal approximation (Hirsch et al., 1993). The standardized test statistic, Z, is calculated as:

$$Z = S/(Var(s))^{\frac{1}{2}} \tag{18}$$

Hisdal et al. (2001) accentuated that the hypothesis H_1 of an upward or downward trend cannot be rejected at a significance level α if $|Z > Z_{(1-\alpha/2)}|$, where $Z_{(1-\alpha/2)}$ is $1-\alpha/2$ quintile of the standard normal distribution. A positive value of Z indicates an upward trend, while a negative value of Z indicates a downward trend. A value of $|Z| > 1.96$ indicates a significant upward/downward trend (at a significance level of $\alpha = 0.05$), and $|Z| > 2.576$ indicates an extremely significant trend (at a significance level of $\alpha = 0.01$) (Zhai and Feng, 2008). In this study, a significance level of $\alpha = 0.05$ is used.

2.4. GCM data

2.4.1. Experimental description

The CSIRO Marine and Atmospheric Research and the Queensland Climate Change Centre of Excellence (QCCCE) are contributing to CMIP5 using the CSIRO Mark 3.6 (Mk3.6), a coupled atmosphere–ocean global climate model. In the present study, the relationships between SPI and RDI in current climate and the future are assessed using simulations and projections of this model. The Mk3.6 climate model is a substantial upgrade from its recent predecessors Mk3.0 and Mk3.5, which were used to contribute to CMIP3. The new Mk3.6 version differs from its recent predecessors by the inclusion of an interactive aerosol scheme, which treats sulfate, dust, sea salt, and carbonaceous aerosol (Rotstayn et al., 2012). It is a coupled atmosphere–ocean model with dynamic sea ice. It also has a soil-canopy scheme with prescribed vegetation properties. The ocean, sea-ice and soil-canopy models are unchanged between Mk3.5 and Mk3.6 (Rotstayn et al., 2013). The ocean model is based on version 2.2 of the Modular Ocean Model, and has 31 vertical levels and horizontal resolution of approximately 0.9375° (latitude) by 1.875° (longitude). The atmospheric model is a spectral model (T63) that utilizes the flux form of the dynamical equations. The atmospheric model has 18 vertical levels and horizontal resolution of approximately 1.875° × 1.875° (spectral T63) (Syktus et al., 2011; Rotstayn et al., 2013).

Recently, the research community has developed a set of scenarios (Representative Concentration Pathways, RCPs) to improve understanding of the complex linkages between human activities and the climate system (van Vuuren et al., 2007), which are used in the Fifth Assessment Report (AR5) of the IPCC and are intended to represent four scenarios of future global development, including greenhouse gas (GHG) emissions, land use, and the resulting atmospheric GHG concentrations, and corresponding atmospheric radiative forcing. The four pathways lead to radiative forcing levels of 8.5, 6, 4.5 and 2.6 W/m^2 by the end of the century. The level of CO_2 concentration at the end of the 21st century and its trajectory during the century vary substantially between RCPs. RCP6.0 and RCP8.5 show monotonically increasing values, while RCP2.6 and RCP4.5 show a peak concentration and stabilized concentration, respectively. Each of the RCPs covers the 1850–2100 period, and extensions have been formulated for the period thereafter (up to 2300). RCP8.5 W/m^2 has been developed by the International Institute for Applied Systems Analysis (IIASA)/Model for Energy Supply Strategy Alternatives and their General Environmental Impact (MESSAGE) modeling team in Austria (Riahi et al., 2007). This corresponds to a world where greenhouse gas emissions continue to rise resulting in atmospheric CO_2 concentration that exceeds 900 ppm by 2100. In the present study, we use the atmospheric data, including precipitation, maximum and minimum temperature, relative humidity, wind speed, and cloud cover for the period 1850–2100 provided by the CSIRO Mk3.6 model based on RCP8.5.

2.4.2. PET assessment

To assess RDI using GCM simulations, PET needs to be calculated based on climatic parameters provided by the above GCM for both historic and future simulations. Reference evapotranspiration (ET_o) is defined as the potential evapotranspiration of a hypothetical surface of green grass of uniform height, actively growing and adequately watered (Xu and Singh, 2005). An accurate estimation of ET is very useful for appropriate water management. ET_o can be computed as a function of weather parameters. Numerous methods, such as temperature-based, radiation-based, and their combinations, have been used to estimate ET_o. The Penman–Monteith (P–M) method is recommended by FAO as the sole method to calculate reference evapotranspiration wherever the required input data are available (Droogers and Allen, 2002). The FAO56-PM model, which is a physically-based approach and incorporates thermodynamic and aerodynamic aspects, has proved to be a relatively accurate method in both humid and arid climates and can be used globally without any need for additional adjustments of parameters (Yin et al., 2008). Therefore, the PM model is used here to assess PET based on CSIRO Mk3.6 data. As per this method, the reference evapotranspiration can be estimated as follows:

$$ET_o = \frac{0.408\Delta(R_n - G) + \gamma[900/(T+273)]\, U_2(e_s - e_a)}{\Delta + \gamma(1 + 0.34\, U_2)} \tag{19}$$

where ET_o is the reference evapotranspiration [mm day^{-1}], Δ is the slope of vapor pressure curve, R_n is the net radiation at the surface [W m^{-2}], G is the soil heat flux density [W m^{-2}], γ is the psychometric constant, T is the mean daily air temperature at the height of 2 m, u_2 is the wind speed at 2-m height, e_s is the saturated vapor pressure, and e_a is the actual vapor pressure [kPa]. The reference surface is assumed to be a flat surface that is completely covered by grass with an assumed uniform height of 0.12 m, a fixed surface resistance of 70 sm^{-1}, and an albedo of 0.23 (Allen et al., 1998).

3. Results and discussion

3.1. Global aridity zones

Fig. 1 shows the distribution of the five aridity zones worldwide based on the UNESCO aridity index (UNESCO, 1979), determined by Asadi Zarch et al. (2014). As the figure shows, the hyper-arid zone is found only in northern Africa and a small part of south-western Asia, southern Africa, and South America, while the remaining four zones are generally found in all the continents, with the humid zone occupying much of the world. Therefore, on one hand, aridity zones are distributed around the world and follow no specific pattern based on latitude, longitude, altitude, and other geographic and topographic factors. On the other hand, however, the literature shows that during recent decades droughts have occurred in almost all the regions. Hence, it can be concluded that occurrence of drought is probable over all the five aridity zones. However, there is a lack of global comparison of droughts occurred in these zones to determine whether drought behaviors and patterns over all the zones are the same or not. This paper, therefore, aims to investigate drought and its trends in different aridity zones. To this end, Fig. 1 is used to delineate the boundaries of the aridity zones for zone-by-zone drought analysis.

3.2. Drought trend analysis: Mann–Kendall test

The Z values derived from the application of the Mann–Kendall (MK) test to the SPI and RDI time series corresponding to each aridity zone for the period 1960–2009 are mapped to show the spatial distribution of drought trends in different aridity zones. Fig. 2 (left) shows the results of the MK test for SPI in the five aridity zones, while Fig. 2 (right) shows the MK results for RDI. As mentioned before, for $\alpha < 0.05$, a Z parameter value of less than -1.96 shows a significant decreasing trend, while a value of more than 1.96 indicates a significant increasing trend, and a value between -1.96 and 1.96 shows no significant trend. It should be noted that, in drought trend analysis based on SPI or RDI, increasing trends indicate a tendency to become more humid, while decreasing trends indicate a tendency to become more dry. The Z parameter values for both SPI and RDI show that, although drought had no significant tendency over large parts of the aridity zones, some areas of all the five aridity zones experienced both significant downward and upward drought trends during the study period. The results obtained for both SPI and RDI are consistent with the results reported in the IPCC Fifth Assessment Report (IPCC, 2013).

Table 2 shows the area of each climatic zone as well as the areal extent of different types of trend (downward, upward, and non-significant) in every climatic zone for both SPI and RDI. The table indicates that climatic feature over half of the world is humid, while hyper-arid is the dominant climate over just 4.5% of the world. Sub-humid, semi-arid and arid zones cover almost the same percentage of area of the world (13–15%). The table also indicates that the prominent observed drought trend tendency in all climatic zones based on both SPI and RDI is the non-significant trend. Based on SPI, the largest non-significant drought trend area is in the semi-arid zone with 87%, while the largest non-significant RDI trend is indicated by the arid zone with more than 89%. Both of the drought indexes show the hyper-arid zone having the lowest tendency of non-significant percentage area: 77.2% with SPI and 80.1% with RDI.

Based on SPI, no significant differences between areal extent of increasing and decreasing trends are observed in the semi-arid and sub-humid zones (less than 1%), while the other zones exhibit remarkable differences. While SPI downward trends are observed in less than 1% of the hyper-arid and arid zones and around 3% of the humid zone, between 12% and 14.5% of these zones exhibit SPI upward trends. On the other hand, based on RDI, except the humid zone, for which both increasing and decreasing trends have almost the same area (around 8%), all the other zones indicate major differences between upward and downward trends. While a significant decreasing trend is found over just around 2% of the hyper-arid and arid zones, 10% of these zones are identified with a significant increasing trend, which reveal that the two zones are becoming wetter. Conversely, the semi-arid and sub-humid zones exhibit more increasing trends (around 10%) than decreasing ones (about 4%), which indicate a tendency toward more dryness. It is interesting to note that the percentage of decreasing trend for RDI is higher than that for SPI in all the aridity zones, while the situation is converse when the increasing trend is considered.

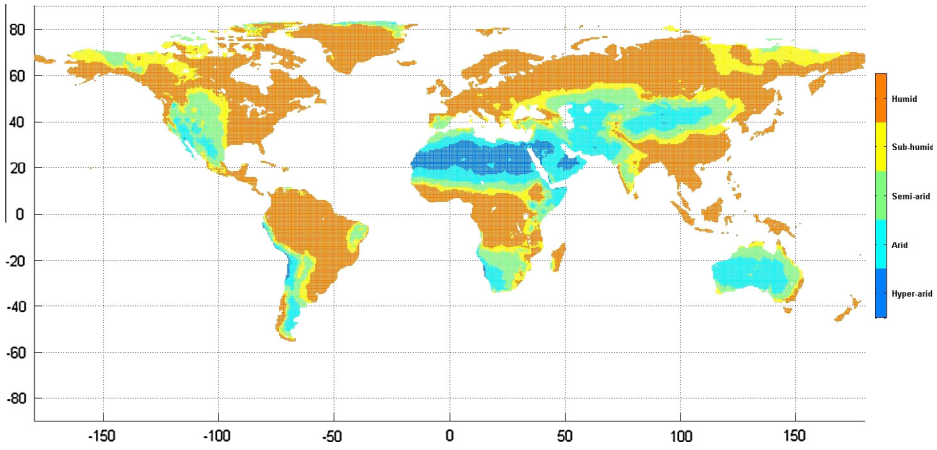

Fig. 1. Global aridity zones (adapted from Asadi Zarch et al., 2014).

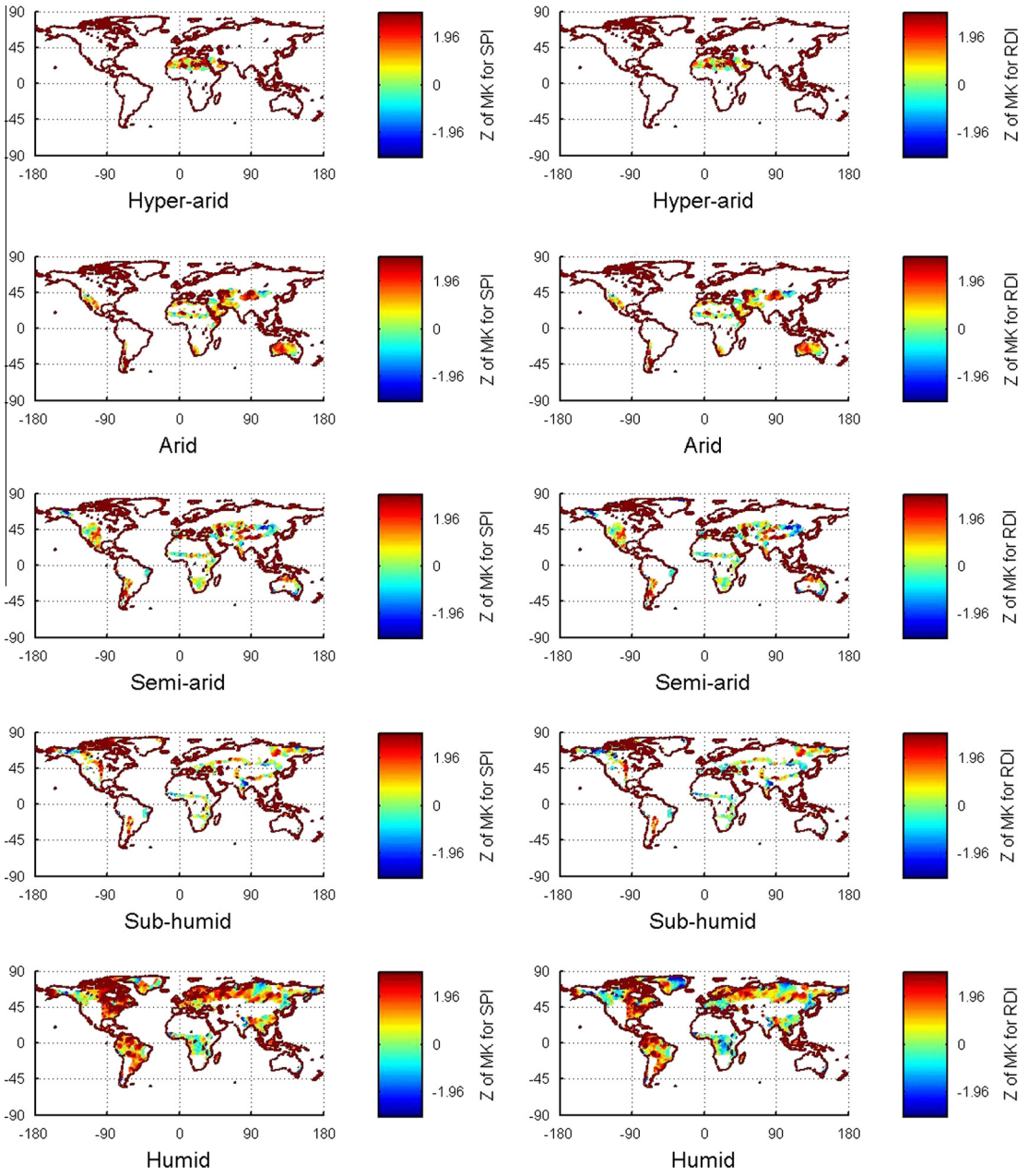

Fig. 2. Mann–Kendall test results for SPI (left) and RDI (right) time series for the period 1960–2009 for five different aridity zones.

Table 2
Area percentage of observed SPI and RDI trends in different climatic zones based on Z values of Mann–Kendall test ($\alpha < 0.05$). $Z > 1.96$ represents a significant increasing trend and $Z < -1.96$ represents a significant decreasing trend.

Climatic zone	Area percentage	Area percentage					
		Non-significant trend		Decreasing trend		Increasing trend	
		SPI	RDI	SPI	RDI	SPI	RDI
Hyper-arid	4.4	77.2	80.1	0.6	1.5	13.1	9.6
Arid	13.0	86.7	89.1	0.8	1.9	12.1	9.0
Semi-arid	14.9	87	85.9	5.6	9.7	6.3	4.3
Sub-humid	13.5	86.2	85.6	6.2	10.4	7.1	4.0
Humid	54.2	80.7	83.8	2.8	8.0	14.5	8.2

3.3. SPI and RDI areal extent

Table 3 shows the year-wise percentage of area covered by drought for the period 1960–2009. Areas with SPI and RDI equal to or less than –1 are considered as areas suffering from drought. Based on Table 1, SPI and RDI values equal to or less than −1 can be classified as moderately dry (−1 to −1.49), severely dry (−1.5 to −1.99) or extremely dry (−2 and less). Based on SPI, the year

Table 3
Global drought areal extent (SPI and RDI <=−1) based on percentage during 1960–2009.

Year	Drought area		Year	Drought area		Year	Drought area		Year	Drought area		Year	Drought area	
	SPI	RDI		SPI	RDI		SPI	RDI		SPI	RDI		SPI	RDI
1960	16.7	16.3	1970	19.8	16.2	1980	18.4	16.8	1990	20.2	22.8	2000	13.2	11.9
1961	18.7	16.1	1971	19.0	17.4	1981	15.3	15.9	1991	16.7	17.4	2001	12.4	14.2
1962	21.8	22.1	1972	27.5	20.9	1982	19.2	16.1	1992	18.7	15.8	2002	14.7	17.1
1963	17.7	14.9	1973	15.4	16.8	1983	22.6	20.3	1993	17.8	15.8	2003	13.0	15.1
1964	19.1	14.1	1974	17.7	16.2	1984	21.7	20.0	1994	14.9	15.4	2004	8.5	10.1
1965	25.6	20.8	1975	16.2	15.9	1985	21.4	18.2	1995	15.7	16.5	2005	11.2	14.5
1966	15.6	11.9	1976	22.1	18.3	1986	20.0	17.2	1996	12.0	10.6	2006	8.2	11.9
1967	16.6	16.0	1977	15.6	13.5	1987	21.5	19.7	1997	11.3	10.7	2007	9.1	11.7
1968	18.0	14.6	1978	16.3	12.9	1988	16.5	18.2	1998	9.7	12.5	2008	9.0	9.7
1969	21.5	17.4	1979	15.3	12.8	1989	17.6	18.1	1999	10.4	10.7	2009	11.9	14.1
SPI average = 16.6%								RDI average = 15.7%						

1965 was the driest year with around 26% under drought condition. However, based on RDI, the year 1990 was the driest year with around 30% of the world covered by drought. The wettest year based on SPI was 2006 (around 8% drought prone areas) and based on RDI was 2008 (around 10% drought prone areas). On average, 16.6% and 15.7% of the world experienced drought annually, according to SPI and RDI, respectively. It is interesting to note that between 1960 and 1997, the drought area percentage of SPI was generally higher than that of RDI, while the converse was the case for the period 1998–2009, except for 2000.

Fig. 3 shows, for instance, the global drought map obtained using SPI (left) and RDI (right) for a dry year (1972) and a wet year (2008). As can be seen, there are some clear differences between the droughts identified by the two indexes for the dry year (1972). This is also consistent with the results in Table 3, with approximately 7% (27.5% versus 20.9%), between the area covered by drought based on SPI and RDI. However, for the wet year (2008), the two indexes generally show similar spatial patterns of drought, with a very small difference between them, i.e. just around 1% (9.0% versus 9.7%). It can be concluded, therefore, that to identify and capture all drought events appropriately, there is a need for drought indexes that optimally use the available information, since droughts do not occur frequently in most regions, especially in the humid and sub-humid zones.

Fig. 4 shows the areal extent of droughts in the five aridity zones over the study period. It is clear that for the period before 1997, except the hyper-arid and arid zones, SPI percentages are more than RDI ones, especially in the sub-humid and humid zones (which totally cover around 68% of the world), while from 1998 onwards, in most cases, drought is generally more extended based on RDI rather than SPI. Therefore, the observed global relationships for drought areal extent, presented by SPI and RDI, shown in Table 3, can be found in most aridity zones. Among the aridity zones, the hyper-arid zone exhibits the highest year-by-year drought area percentage fluctuations and the humid zone presents the lowest. Therefore, to reduce the impacts of drought, especially in the hyper-arid and arid zones that naturally face water scarcity, a better knowledge of droughts, through improving our understanding of the characteristics and relationships of drought, is necessary.

3.4. GCM simulation and projections

The SPI and RDI are calculated for the periods 1850–2005 and 2006–2100 using past and future simulations from CSIRO Mk3.6 based on RSP8.5. To assess RDI, global PET is calculated using the Penman–Monteith method based on CSIRO Mk3.6 climatic parameters for 1850–2100. Fig. 5, for example, presents the classified SPI

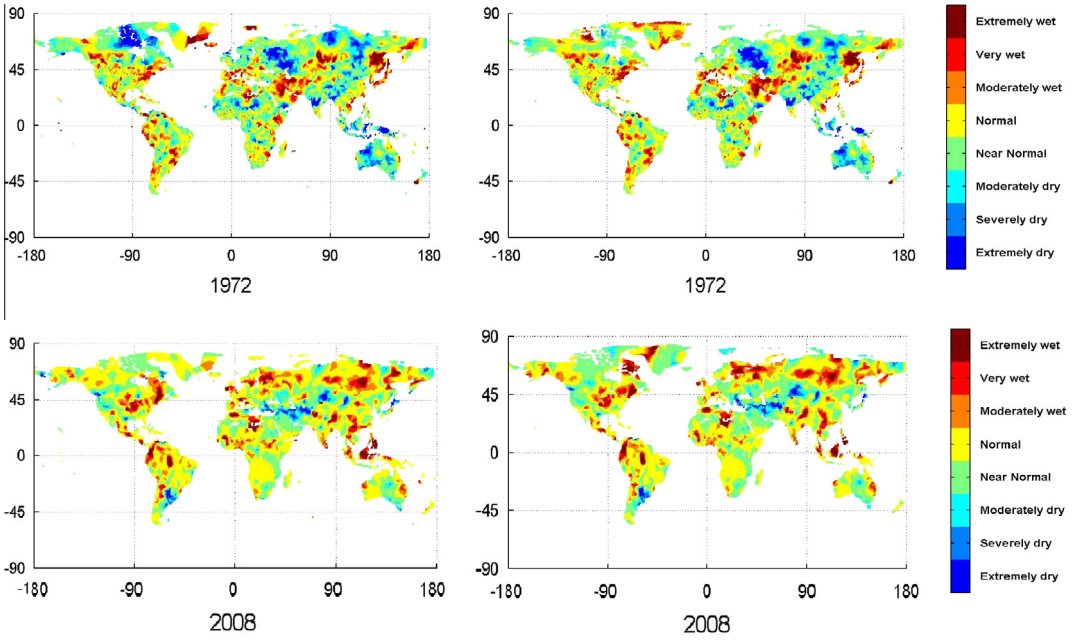

Fig. 3. Global drought map based on SPI (left) and RDI (right): a dry year (1972) and a wet year (2008).

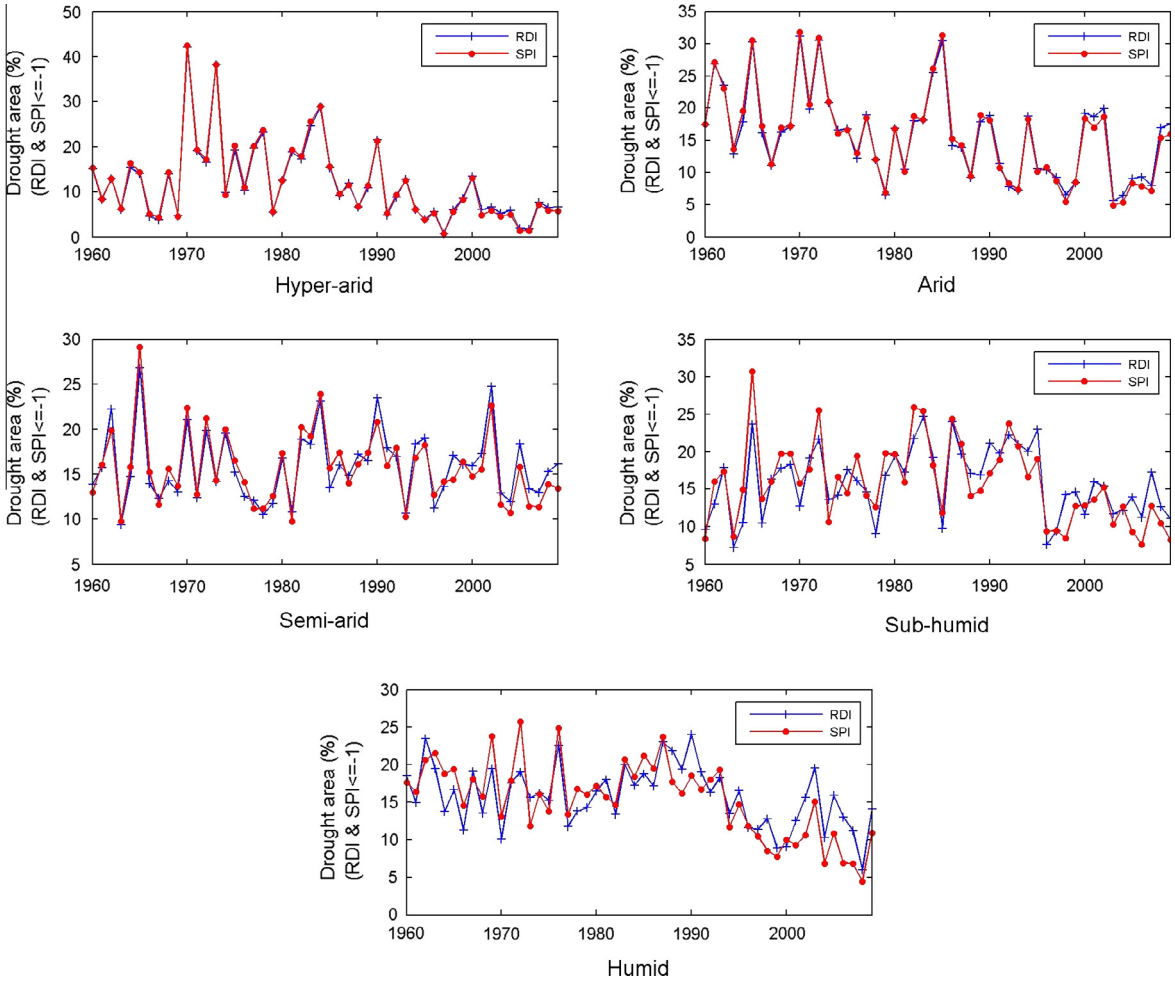

Fig. 4. Drought areal extent (SPI and RDI <=–1) based on percentage for five aridity zones during 1960–2009.

and RDI values (based on Table 1) for the year 1850, the first year of the study period of the current climate. The maps present major similarities between SPI and RDI, and there exist no remarkable changes between them in many parts around the globe.

Fig. 6, for example, presents the global SPI and RDI drought classes for the year 2100, the last year of the study period of future climate using simulations of the CSIRO Mk3.6 model. Unlike 1850, when there is a significant agreement in the drought classes obtained using the two indexes, the SPI and RDI indexes for the year 2100 clearly show different drought classes in considerable parts of the world. In 2100, SPI shows that some regions are more wet than those shown by the RDI, but this pattern may also be different for the other years.

Although Figs. 5 and 6 exhibit a reduction in agreement between SPI and RDI from 1850 to 2100, more comprehensive comparisons are required to verify if this is indeed the case. Since SPI and RDI values should be classified based on Table 1 to be more usable in water resources assessment and management, including for drought classification, a drought class comparison between the two indexes is done for three separate periods: 1951–2000, 2001–2050, and 2051–2100. To this end, SPI and RDI are calculated for each of the three periods separately. Therefore, there is one SPI and one RDI time series for each land grid cell with the time series including 50 annual drought values, and the calculations are carried out for each grid cell for SPI and RDI separately. As mentioned earlier (see Table 1), SPI and RDI have eight drought classes. In general, if the two indexes do not show the same drought class(es), they may probably exhibit the adjusted classes, although in some cases the difference may even be more than one class. To highlight this, a weighted drought class comparison, which calculates the difference based on the number of drought classes between the two classes added by one, is applied. It is obvious that if the indexes show the same class(es), the weighting is not applied and the difference is considered as zero. Based on the weighted drought class comparison method, the difference is one for adjacent classes, and is more than one for farther classes. For example, the difference is one if one of the indexes shows drought as severely dry and the other as moderately dry, while if one exhibits severely dry and normal is presented by the other, then the difference is three. For easy interpretation of the results for the three periods, the class change between the two indexes for each period is averaged. To find out whether the drought class difference between SPI and RDI has increased with time or not, the averaged values for each of the above three periods are mapped in Fig. 7. The figure clearly shows that the class difference between SPI and RDI increases from the first period toward the third one. The mean value for 1951–2000, 2001–2050, and 2051–2100 is 0.246, 0.264, and 0.373, respectively.

It should be noted that Fig. 7 only shows the class difference between SPI and RDI but provides no knowledge as to whether one of the indexes mostly shows more wet classes or often indicates more dry or there is no any specific pattern. This is addressed in Fig. 8. To determine the effects of nonstationary climate on the relationships between droughts identified by SPI and RDI during

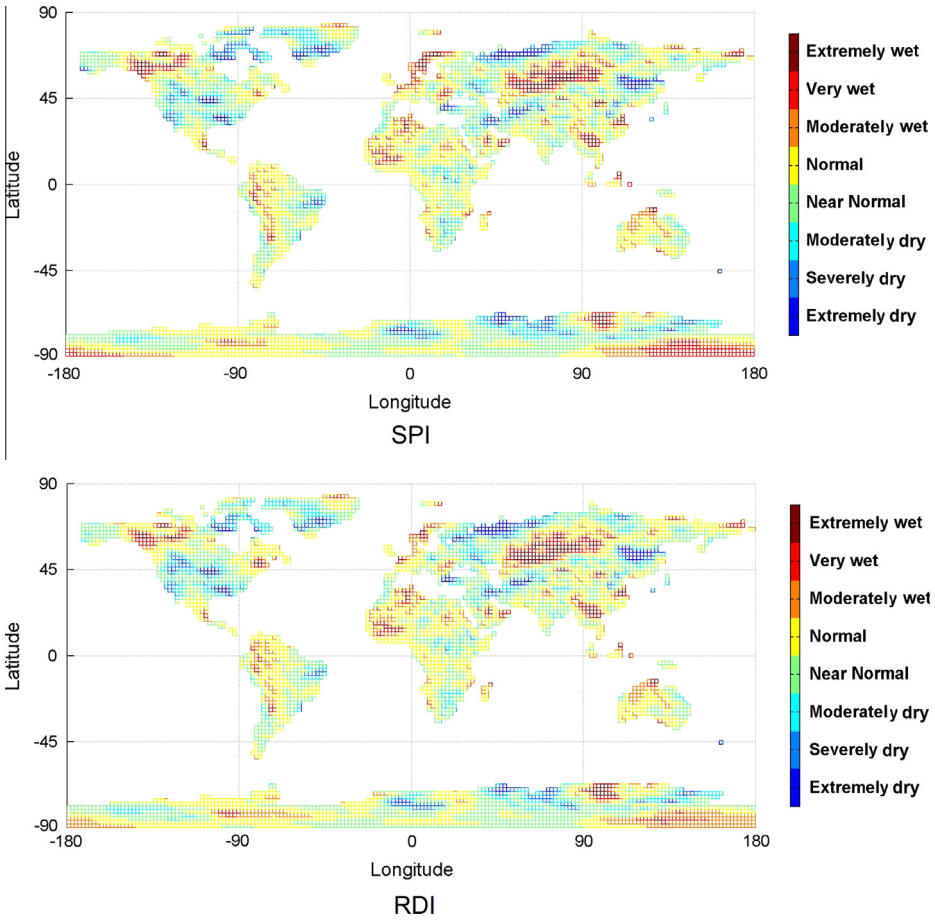

Fig. 5. Global drought map for 1850 for SPI and RDI based on CSIRO Mk3.6 simulations.

1951–2100, the average drought class difference for the three periods (1951–2000, 2001–2050, and 2051–2100) is presented in Fig. 8. The class difference is presented for two situations: (1) SPI class is greater (i.e. more wet) than RDI; and (2) RDI class is greater (i.e. more dry) than SPI. Since SPI and RDI classes can be same for some grids, for better illustration, grids having no drought class difference during each of the three periods are excluded from the figure. The drought class difference calculation is done for each grid for each year separately and the values are then averaged over 50 years of each of the three periods. The results indicate not only that most parts of the world experienced different SPI and RDI drought classes, but also that SPI indicates more humid (or dry) class in some years while RDI does in some other years. Therefore, any assumption or concern that one of the indexes may show more dry (or more humid) than the other in most years may not be valid.

4. Discussion

Analysis of trends in drought for the period 1960–2009 indicates that SPI and RDI are in good agreement in the hyper-arid and arid zones (Fig. 2). However, in the semi-arid and sub-humid zones, SPI indicates no clear trend, while RDI shows more downward trends. In the humid zone, SPI shows that the zone is becoming significantly more humid, while there are approximately same area percentages of RDI increasing and decreasing tendencies. On the other hand, in all the zones, RDI shows greater area percentage of decreasing and less of increasing trend than SPI. These results lead to two important points: (1) the agreement between SPI and RDI reduces from the hyper-arid zone toward the humid zone; and (2) when the drought tendencies are different between the indexes, RDI shows more trends toward dryness than SPI does.

About the first point, the significant fluctuation in the spatio-temporal distribution of precipitation in the dry regions may be the cause of the observed high similarity between SPI and RDI in the hyper-arid and arid zones. Asadi Zarch et al. (2014) report that the average coefficient of variation (CV) of precipitation for the period 1960–2009 is 0.66, 0.38, 0.25, 0.21, and 0.17 for the hyper-arid, arid, semi-arid, sub-humid, and humid zones, respectively. Therefore, not only the arid zones (hyper-arid and arid) receive low precipitation rates but also precipitation presents a high range of variability in such zones. Therefore, in the arid zones, while PET is not supposed to vary remarkably, RDI changes with respect to precipitation variations and is mostly a derivative of precipitation rather than PET. It is obvious that this helps RDI to behave almost same as SPI, which considers just precipitation to assess droughts. For the remaining zones, it seems that as the CV of precipitation decreases, PET plays a more important role in characterizing the occurrence of drought based on RDI. Therefore, SPI and RDI indicate less agreement in these zones.

To address the second point, the land area affected by drought during 1960–2009 is presented based on percentage of the global area (Table 2) and in the five climatic zones (Fig. 4). Droughts have affected larger areas since the 1970s (IPCC, 2007). In studying drought characteristics, it is obvious that the extent of droughts varies from one region to another. From 1960 to 1987, SPI shows a higher area percentage of drought than RDI except in three years (1962, 1973, and 1981), while, conversely, from 1988 to 2000, RDI values mostly show higher percentage area of drought than SPI ones. Finally, all years over the period 2000–2009 show more

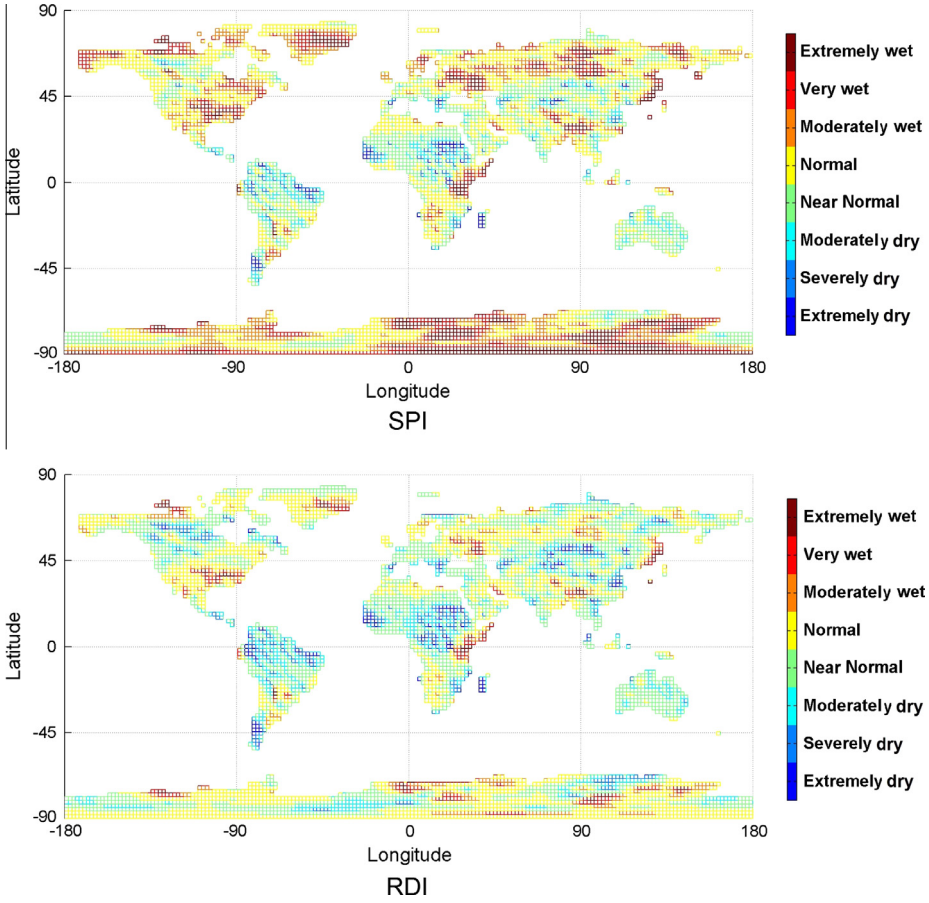

Fig. 6. Global drought map for 2100 for SPI and RDI based on CSIRO Mk3.6 simulations.

RDI drought percentage than SPI. The results are almost the same for all the five climatic zones (Fig. 4). As mentioned earlier, the only difference between SPI and RDI is that RDI takes into consideration PET too in addition to precipitation. Remarkable rising trends of temperature in recent decades have caused positive trends of PET in considerable parts of the world and have resulted in higher drought prone areas indicated by RDI than SPI.

Next, the period 1962–2009 is divided to 4 sub-periods (1962–1973, 1974–1985, 1986–1997, and 1998–2009), and the mean global temperature is averaged for these sub-periods. The results indicate the average of mean global temperature as 4.72 °C, 4.92 °C, 5.30 °C, and 5.73 °C for the four sub-periods, respectively. As temperature has increased within the four sub-periods above, the degree of greatness of SPI when compared to RDI has decreased. Based on SPI, the average extent of area under drought is 19.80%, 18.48%, 16.91%, and 10.94% for the four sub-periods, respectively. The RDI, however, shows the areal extent as 16.93%, 16.41%, 16.52%, and 12.79% for the four sub-periods, respectively. While the difference between the indexes is relatively small in the third sub-period, RDI is greater than SPI in the last one. Therefore, on one hand, the average temperature, and as a result PET, in the fourth sub-period is remarkably higher than the previous ones. On the other hand, not only SPI, which takes only precipitation into account, but also RDI, which takes also PET into consideration, indicate 1998–2009 as the wettest sub-period. To address this, the average of mean global precipitation for all the sub-periods is estimated and found to be 683.57 mm, 685.95 mm, 683.92 mm, and 699.29 mm for the four sub-periods, respectively. Therefore, since the average precipitation in the fourth sub-period (1998–2009) is considerably higher than the

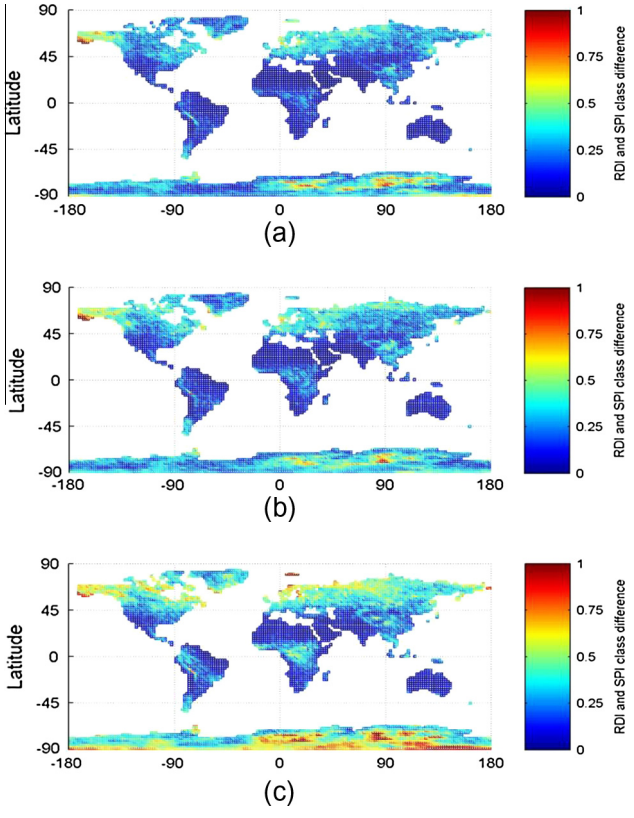

Fig. 7. Average drought class difference between SPI and RDI for periods (a) 1951–2000, (b) 2001–2050 and (c) 2051–2100.

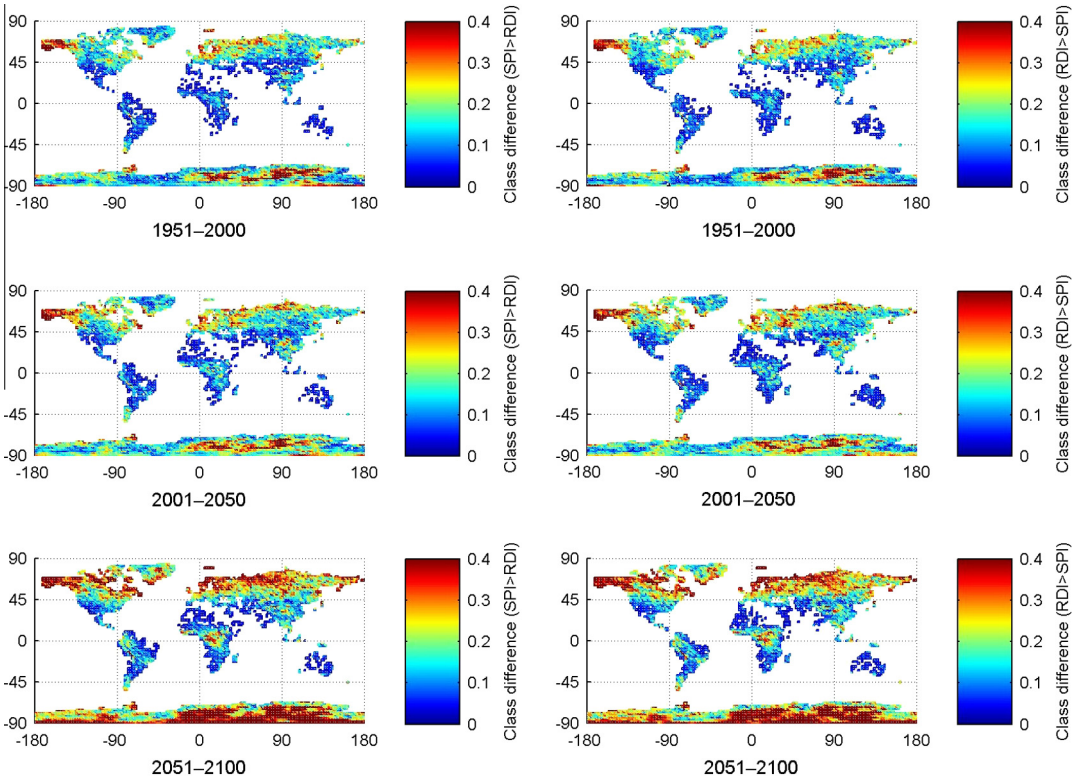

Fig. 8. Average drought class difference between SPI and RDI when SPI > RDI (left) and RDI > SPI (right) for periods 1951–2000, 2001–2050 and 2051–2100.

other ones, areal extent of drought has decreased in this sub-period, despite the higher PET rates resulted by high temperatures.

Based on the present results, although general similarities can be found between SPI and RDI in the five aridity zones for the past, there exist also some differences that cannot be ignored. Since drought occurs when there exists a deficit in available moisture relative to its normal, a decrease in precipitation or increase in ET or both may result in drought. The rise in global CO_2 concentration during the last few decades has caused higher temperatures and resulted in an increase in the global atmospheric demand for moisture. The PET may be one of the best representatives of atmospheric water demand and, therefore, its inclusion in a drought index should improve not only the accuracy of the index in detecting droughts but also in representing the sensitivity of the index to climate changes to capture the related impacts. Since the assumption of stationarity in traditional hydrologic considerations may no longer be valid under climate change conditions (Milly et al., 2008), especially in the context of clear positive trends of temperature in the recent past, selecting a drought index that is able to capture the resultant changes in drought occurrence can help to monitor drought trends properly.

For the future, both precipitation and ET are expected to change with global warming at different scales across the globe. Future climate changes, even under conservative scenarios, are likely to cause further increases in mean temperature (about 2–4 °C globally) (Seager et al., 2007). Therefore, the necessary characteristics of drought indexes, mentioned above, also apply for projection of future droughts. Consequently, it is vital to use a drought index that is sensitive to global warming. Drought events in the future should be predicted to investigate how drought might change in future and to plan for their impacts and associated damages. Climate models, which are developing rapidly, are the most useful tools to anticipate future climate changes. Therefore, we have used the twentieth and twenty-first century simulations of CSIRO Mk3.6 model (with RCP8.5) to calculate SPI and RDI. The simulations have been used to assess the indexes in two periods, 1850–2005 and 2006–2100, as historic and future droughts, respectively (Figs. 5–8). Comparing of drought maps of the first year of the historic period (year 1850) indicates significant similarities between SPI and RDI (Fig. 5), while substantial differences can be found in the last year of the future period of comparison (year 2100) (Fig. 6). The results for these two years lead to the interpretation that agreement between SPI and RDI is affected and decreases remarkably between 1850 and 2100. While this may just be considered as a coincidence as well, more robust findings, through a weighted drought class comparison between the two indexes for three study periods, 1951–2000, 2001–2050, and 2051–2100 (Figs. 7 and 8), also indicate an increase in difference between SPI and RDI. Therefore, it can be concluded that, in the face of global warming in the future, PET, which is an important component in the hydrologic cycle and shows the atmospheric demand for moisture, should no longer be ignored in drought forecasting.

5. Conclusions

In recent decades, the impacts of frequent drought occurrence are aggregated by the rise in water demand due to population growth and climate change effects, e.g. an increase in evapotranspiration in regions with rising temperatures. Therefore, understanding and qualifying drought occurrence and its consequences on agricultural production, hydrologic cycle, and ecosystems is of particular importance. It is obvious that determining the drought hazards is quite difficult and complicated, but drought monitoring using drought indexes often serves as an important base. In regards to drought occurrence in all the climatic zones, the objective of this study was to assess the annual spatio–temporal variation trends of drought events in different aridity zones for the past and also to

obtain useful information for future drought assessment. Two drought indexes, namely SPI and RDI, were used in the analysis.

The results generally indicate that the percentage of drought prone areas estimated by SPI is mostly higher than RDI for the period prior to 1998, while it is the converse for the period after 1998. Based on SPI and RDI, the hyper-arid and arid zones are estimated to become slightly more humid, while the results provided by the two indexes for the other zones are not same. While the areal extent of RDI decreasing trend is higher than that of SPI in all the zones, the extent of RDI increasing trend is, conversely, lower than that of SPI. The results also suggest that the agreement between SPI and RDI in the arid zones is higher when compared to that in the humid zones. In the semi-arid, sub-humid, and humid zones, where the drought trends are identified to be different between the two indexes, RDI shows more trends toward dryness than SPI.

Differences between SPI and RDI are expected to continue in the future, as reflected by the results from the comparison of class difference between the indexes using the current and future simulations of a CMIP5 model. The results indicate that SPI, which considers no atmospheric demand parameters, may not be capable of identifying future droughts under an increasing temperature trend. Therefore, although SPI is one of the most popular drought indexes, it is, to some extent, constrained in the projection of droughts under a changing climate. Although more studies are needed to find out the most appropriate drought index for conditions under climate change, a particular advantage of RDI is that it considers, in addition to precipitation, potential evapotranspiration (PET), which is an essential parameter for detection of droughts and their characteristics under increased greenhouse gas concentrations. To this end, study of seasonal characteristics of droughts in aridity zones may also shed additional light on the performance of SPI and RDI. Investigations in these directions are underway, details of which will be reported elsewhere.

Acknowledgments

The Australian Research Council (ARC) is acknowledged for funding support for part of the research reported here. Bellie Sivakumar acknowledges the financial support from ARC through the Future Fellowship grant (FT110100328). We thank Ashok Mishra and the two anonymous reviewers for their positive and constructive comments on an earlier version of this manuscript.

References

Abramowitz, M., Stegun, A., 1965. Handbook of Mathematical Functions: with Formulas, Graphs, and Mathematical Tables. Dover Publications Inc., New York.
Allen, R.G., Pereira, L.S., Raes, D., Smith, M., 1998. Crop evapotranspiration. FAO Irrigation and Drainage Paper 56, Food and Agriculture Organization, Rome.
Asadi Zarch, M.A., Sivakumar, B., Sharma, A., 2014. Assessment of global aridity change. J. Hydrol., submitted for publication.
Belda, M., Holtanová, E., Halenka, T., Kalvová, J., 2014. Climate classification revisited: from Köppen to Trewartha. Clim. Res. 59, 1–13.
Chen, J., Chan, F.P., 2007. A preliminary drought mitigation plan for Hong Kong. MODSIM 2007, International Congress on Modelling and Simulation, pp. 1492–1498.
Damberg, L., 2013. Analysis of Trends and Patterns of Droughts Using Satellite Data and Climate Model Simulations. Master thesis. Lund University.
Droogers, P., Allen, R.G., 2002. Estimating reference evapotranspiration under inaccurate data conditions. Irrig. Drain. Syst. 16, 33–45.
Gocic, M., Trajkovic, S., 2014. Spatiotemporal characteristics of drought in Serbia. J. Hydrol. 510, 110–123.
Hamed, K.H., 2009. Exact distribution of the Mann–Kendall trend test statistic for persistent data. J. Hydrol. 365, 86–94.
Harris, I., Jones, P.D., Osborn, T.J., Lister, D.H., 2014. Updated high-resolution grids of monthly climatic observations – the CRU TS3.10 Dataset. Int. J. Climatol. 34, 623–642.
Hirsch, R., Helsel, D., Cohn, T., Gilroy, E., 1993. Statistical analysis of hydrologic data. In: Maidment, D. (Ed.), Handbook of Hydrology. McGraw-Hill, New York.
Hisdal, H., Stahl, K., Tallaksen, L.M., Demuth, S., 2001. Have streamflow droughts in Europe become more severe or frequent? Int. J. Climatol. 21, 317–333.
IPCC, 2007. Climate change 2007: Synthesis Report. Contribution of Working Groups I, II and III to the Fourth Assessment Report of the Intergovernmental Panel on Clim. Change, IPCC, Geneva, Switzerland.
IPCC, 2013: Summary for Policymakers. In: Climate Change 2013: The Physical Science Basis. Contribution of Working Group I to the Fifth Assessment Report of the Intergovernmental Panel on Climate Change. In: Stocker, T.F., Qin, D., Plattner, G.-K., Tignor, M., Allen, S.K., Boschung, J., Nauels, A., Xia, Y., Bex, V., Midgley, P.M., (Eds.), Cambridge University Press, Cambridge, UK.
Johnson, F.M., Sharma, A., 2010. A comparison of Australian open water body evapotranspiration trends for current and future climates estimated from Class A evaporation pans and general circulation models. J. Hydrometeorol. 11 (1), 105–121.
Kao, S.-C., Govindaraju, R.S., 2010. A copula-based joint deficit index for droughts. J. Hydrol. 380 (1–2), 121–134.
Kendall, M.G., 1975. Rank Correlation Methods. Griffin, London, UK.
Mann, H.B., 1945. Nonparametric tests against trend. Econometrica 13, 245–259.
McKee, T.B., Doesken, N.J., Kleist, J., 1993. The relationship of drought frequency and duration to time scales. In: Eighth Conference on Applied Climatology. American Meteorological Society, Anaheim, CA, pp. 179–186.
Milly, P.C.D., Betancourt, J., Falkenmark, M., Hirsch, R.M., Kundzewicz, Z.W., Lettenmaier, D.P., Stouffer, R.J., 2008. Stationarity is dead: whither water management? Science 319, 573–574.
Mishra, A.K., Singh, V.P., 2009. Analysis of drought severity-area-frequency curves using a general circulation model and scenario uncertainty. J. Geophys. Res.-Atmos. 114, D06120. http://dx.doi.org/10.1029/2008JD010986.
Mishra, A.K., Singh, V.P., 2010. A review of drought concepts. J. Hydrol. 391 (1–2), 202–216.
Mishra, A.K., Singh, V.P., 2011. Drought modeling: a review. J. Hydrol. 403 (1–2), 157–175.
Özger, M., Mishra, A.K., Singh, V.P., 2010. Estimating Palmer drought severity index using a wavelet fuzzy logic model based on meteorological variables. Int. J. Climatol. 31 (13), 2021–2032.
Palmer, W.C., 1965. Meteorological drought. Research Paper No. 45, U.S. Department of Commerce Weather Bureau, Washington, D.C.
Riahi, K., Gruebler, A., Nakicenovic, N., 2007. Scenarios of long-term socio-economic and environmental development under climate stabilization. Technol. Forecasting Social Change 74, 887–935.
Rotstayn, L.D., Jeffrey, S.J., Collier, M.A., Dravitzki, S.M., Hirst, A.C., Syktus, J.I., Wong, K.K., 2012. Aerosol- and greenhouse gas-induced changes in summer rainfall and circulation in the Australasian region: a study using single-forcing climate simulations. Atmos. Chem. Phys. 12, 6377–6404.
Rotstayn, L.D., Collier, M.A., Chrastansky, A., Jeffrey, S.J., Luo, J.-J., 2013. Projected effects of declining aerosols in RCP4.5: unmasking global warming? Atmos. Chem. Phys. 13, 10883–10905. http://dx.doi.org/10.5194/acp-13-10883-2013.
Salas, J.D., 1993. Analysis and modeling of hydrologic time series. In: Maidment, D.R. (Ed.), Handbook of Hydrology. McGraw Hill, New York, pp. 19.1–19.72.
Sanderson, M. (Ed.), 1992. UNESCO Sourcebook in Climatology for Hydrologists and Water Resource Engineers. UNESCO, Paris.
Seager, R., Ting, M., Held, I., Kushnir, Y., Lu, J., Vecchi, G., Huang, H.P., Harnik, N., Leetmaa, A., Lau, N.C., Li, C., Velez, J., Naik, N., 2007. Model projections of an imminent transition to a more arid climate in southwestern North America. Science 316, 1181–1184.
Shafer, B.A., Dezman, L.E., 1982. Development of a Surface Water Supply Index (SWSI) to assess the severity of drought conditions in snowpack runoff areas. In: Proceedings of the Western Snow Conference. Colorado State University, Fort Collins CO., pp. 164–175.
Sivakumar, B., 2011a. Water crisis: from conflict to cooperation – an overview. Hydrol. Sci. J. 56 (4), 531–552.
Sivakumar, B., 2011b. Global climate change and its impacts on water resources planning and management: assessment and challenges. Stoch. Environ. Res. Risk Assess. 25 (4), 583–600.
Syktus, J., Jeffrey, S., Rotstayn, L., Wonga, K., Toombs, N., Dravitzki, S., Collier, M., Hamalainena, C., Moeseneder, C., 2011. The CSIRO-QCCCE contribution to CMIP5 using the CSIRO Mk3.6 climate model. In: 19th International Congress on Modelling and Simulation, Perth, Australia, 12–16 December.
Tallaksen, L.M., van Lanen, H.A.J., 2004. Hydrological Drought: Processes and Estimation Methods for Streamflow and Groundwater. Developments in Water Science, vol. 48. Elsevier, Amsterdam, p. 579.
Taylor, K.E., Stouffer, R.J., Meehl, G.A., 2012. An overview of CMIP5 and the experiment design. Bull. Am. Meteorol. Soc. 93, 485–498.
Thom, H.C.S., 1958. A note on gamma distribution. Mon. Weather Rev. 86, 117–122.
Tsakiris, G., Vangelis, H., 2005. Establishing a drought index incorporating evapotranspiration. Eur. Water. 9 (10), 3–11.
Tsakiris, G., Nalbantis, I., Pangalou, D., Tigkas, D., Vangelis, H., 2008. Drought meteorological monitoring network design for the Reconnaissance Drought Index (RDI). In: 1st International Conference "Drought Management: Scientific and Technological Innovations". Zaragoza, Spain. 12–14 June 2008. pp. 57–62.
UNESCO, 1979. Map of the world distribution of arid regions. Explanatory note, Man and Biosphere MAB.
van Vuuren, D., den Elzen, M., Lucas, P., Eickhout, B., Strengers, B., van Ruijven, B., Wonink, S., van Houdt, R., 2007. Stabilizing greenhouse gas concentrations at low levels: an assessment of reduction strategies and costs. Clim. Change. 81, 119–159.
Xu, C.Y., Singh, V.P., 2005. Evaluation of three complementary relationship evapotranspiration models by water balance approach to estimate actual regional evapotranspiration in different climatic regions. J. Hydrol. 308, 105–121.

Yang, H.B., Yang, D.W., 2012. Climatic factors influencing changing pan evaporation across China from 1961 to 2001. J. Hydrol. 414–415, 184–193.
Yin, Y., Wu, S., Zheng, D., Yang, Q., 2008. Radiation calibration of FAO56 Penman–Monteith model to estimate reference crop evapotranspiration in China. Agr. Water Manage. 95, 77–84.
Yu, Y., Zou, S., Whittemore, D., 1993. Non-parametric trend analysis of water quality data of rivers in Kansas. J. Hydrol. 150, 61–80.
Zhai, L., Feng, Q., 2008. Spatial and temporal pattern of precipitation and drought in Gansu Province, Northwest China. Nat. Hazards. 49, 1–24.